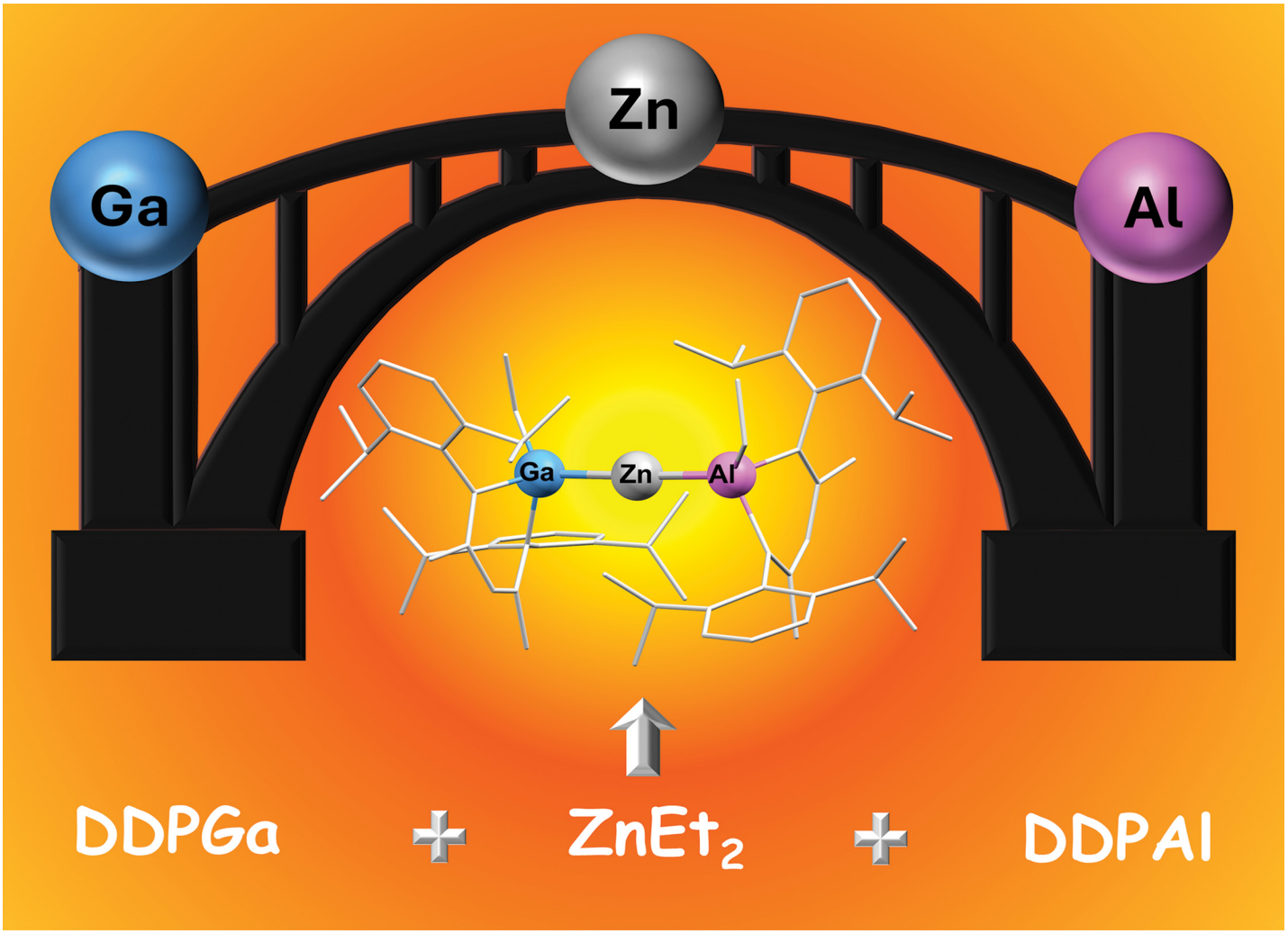

Showcasing research from Professor Stephan Schulz's laboratory, Institute of Inorganic Chemistry, University of Duisburg-Essen, Essen, Germany, and the Center for Nanointegration Duisburg-Essen (CENIDE), Duisburg, Germany.

Synthesis and reactivity of acyclic heterotrinuclear metal complexes

Stepwise oxidative addition of $ZnEt_2$ with heavier carbene analogues affords acyclic heterotrinuclear complexes bearing three different metals. Structural, spectroscopic, and computational analyses highlight unique Ga–Zn–Al/Si bridges and reveal cooperative reactivity toward Lewis acids, NH_3, and alcohols.

Image reproduced by permission of Stephan Schulz from *Chem. Commun.*, 2025, **61**, 16774.

As featured in:

See Stephan Schulz *et al.*, *Chem. Commun.*, 2025, **61**, 16774.

ROYAL SOCIETY OF CHEMISTRY

rsc.li/chemcomm

Registered charity number: 207890

ChemComm

COMMUNICATION

View Article Online
View Journal | View Issue

Cite this: *Chem. Commun.*, 2025, **61**, 16774

Received 27th June 2025,
Accepted 24th September 2025

DOI: 10.1039/d5cc03627e

rsc.li/chemcomm

Synthesis and reactivity of acyclic heterotrinuclear metal complexes

Rajata Kumar Sahoo,[a] Christoph Wölper,[a] Joost Möbius[a] and Stephan Schulz *[ab]

Heterobimetallic complexes [L¹(Et)MZn(Et)] (M = Al 1a, Ga 1b; L¹ = {HC(C(CH₃)N(Dipp))₂}, Dipp = 2,6-iPr₂-C₆H₃) and heterotrinuclear complexes [L¹(Et)GaZnM(Et)L¹] (M = Al 2a, Ga 2b) and [L¹(Et)GaZnSi(Et)L²] (2c; L² = {N(Dipp)C(CH₃)CHC(CH₂)(N(Dipp)}) were synthesized by stepwise oxidative addition reactions of ZnEt₂ with heavy carbene analogues and fully characterized including single crystal X-ray diffraction (sc-XRD). Reactions of 2c with B(C₆F₅)₃, NH₃ and PhCH₂OH are also reported.

Multimetallic complexes have been intensively studied in small molecule activation reactions and catalytic reactions.[1] Homo- and heterobimetallic complexes are also of interest, since they potentially offer beneficial cooperative effects between the metal centres,[2] enabling activation of inert bonds.[3] For example, cooperative C–F bond activation reactions were reported for a bis-gallanediyl and a Zn–Al compound.[4,5] Acyclic trimetallic complexes are expected to be even more interesting,[6] but are limited to acyclic homonuclear (**I**,[7] **II**,[8] **III**,[9] Fig. 1) and heterobinuclear complexes. These are often obtained from oxidative addition of metal complexes bearing M–M or M–X bonds (X = group 13–17 elements) to monovalent group 13 diyls,[10] *i.e.*, [L¹Ga(Et)]₂InEt **IV** (L¹ = HC[C(CH₃)N(Dipp)]₂, Dipp = 2,6-iPr₂-C₆H₃) was synthesized by twofold oxidative addition of InEt₃ to L¹Ga,[11] Zn[Al(η²-Cp*)N(SiMe₃)₂]₂ **V** by reaction of Cp*Al and Zn[N(SiMe₃)₂]₂,[12a] and [L¹(X)GaZnGa(X)L¹] (X = Me **VI**, H **VII**) by reaction of L¹Ga with Zn–X bonds.[12b,c] While this work was in progress, Crimmin *et al.* reported the synthesis of acyclic L¹M(ZnCp*)₂ (**VIII**) and L²Si(ZnCp*)₂ (**IX**) by reactions of L¹M and L²Si (L² = {DippNC(CH₃)C(H)C(CH₂)(NDipp}) with Cp*₂Zn₂,[13a] while reactions of Cp*₂Zn₂ with transition metal complexes gave cyclic complexes.[13b,c] In addition, Hg(ZnL¹)₂ was synthesised by salt elimination reaction.[14] In contrast, acyclic heterotrinuclear complexes containing three different metals have not yet been reported, most likely due to the challenging synthetic routes, *i.e.*, the reaction of three different metal precursors is often accompanied by side reactions. Herein, we report the synthesis of heterotrinuclear complexes containing three different metal atoms *via* stepwise oxidative addition of ZnEt₂ to L¹M and L²Si, respectively, and reactions of compound **2c** with B(C₆F₅)₃, NH₃, and PhCH₂OH.

Equimolar reactions of ZnEt₂ and L¹M (M = Al, Ga) in benzene or toluene solution gave donor-free compounds [L¹(Et)MZnEt] (M = Al **1a**, M = Ga **1b**) (Scheme 1) in high yields.

The formation of compounds **1a–b** was confirmed by ^{1}H NMR spectroscopy, showing shifts in the methine resonance of the ligand backbone from 5.18 ppm (L¹Al)[15] to 4.82 ppm (**1a**) and from 5.19 ppm (L¹Ga)[16] to 4.77 ppm (**1b**) in C_6D_6. The ^{1}H and ^{13}C{1H} NMR spectra also show characteristic resonances for the M–Et and Zn–Et groups, respectively. Variable-temperature (VT) ^{1}H NMR studies (−30 °C to 40 °C) were performed to investigate the thermal stability of compound **1a** (Fig. S6–S8). **1a** started to decompose at 20 °C with formation of **1a–Et₂** along with a dark grey precipitate of metallic zinc. ^{1}H, ^{13}C{^{1}H} and ^{27}Al{^{1}H} NMR spectra of **1a** were therefore recorded in toluene-d_8 at −30 °C (Fig. S1–S3). A solution of **1b** in C_6D_6 also decomposed to compound **1b–Et₂** and metallic zinc within 18 h at room temperature (Scheme 1).

Single crystals of **1a** and **1b** were obtained from *n*-hexane solutions upon storage at −30 °C. They crystallize in the

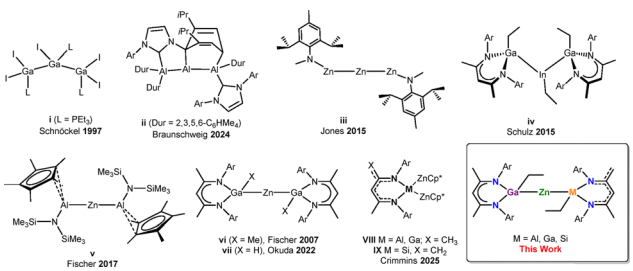

Fig. 1 Selected structurally characterized acyclic homo-and hetero-metallic trinuclear complexes (Ar = Dipp = 2,6-iPr₂C₆H₃).

[a] *Institute of Inorganic Chemistry, University of Duisburg-Essen Universitätsstr.5–7, 45141 Essen, Germany. E-mail: stephan.schulz@uni-due.de*

[b] *Center for Nanointegration Duisburg-Essen (CENIDE), University of Duisburg-Essen Carl-Benz-Straße 199, 47057 Duisburg, Germany*

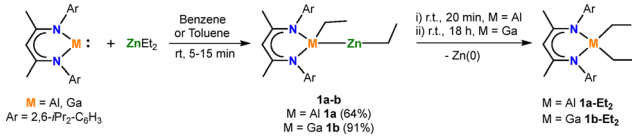

Scheme 1 Reaction of L^1M (M = Al, Ga) with $ZnEt_2$.

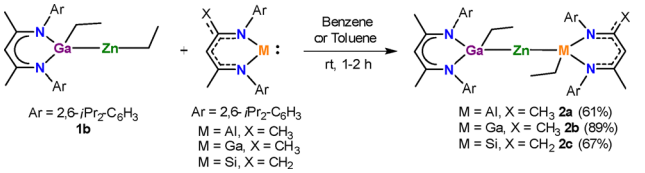

Scheme 2 Synthesis of **2a–c** by oxidative addition of **1b** to heavier carbene analogues.

orthorhombic space groups *Pnma* (**1a**) and $P2_12_12_1$ (**1b**), and their molecular structures in the solid state are shown in Fig. 2. The Al/Ga atoms in **1a** and **1b** exhibit distorted tetrahedral geometries, whereas the Zn atoms are almost linearly coordinated. The Al1–Zn1 bond length in **1a** (2.4908(10) Å) is slightly longer than the Al–Zn bonds in $[L^1(Et)AlZnL^3]$ (2.488(1) Å)[3a] and in $[L^1(Br)AlZn(Br)(tmeda)]$ (2.471(1) Å),[17] and the Ga1–Zn1 bond length in **1b** (2.4265(4) Å) is shorter than the Ga–Zn bond length in $[L^1(H)GaZn(H)(tmeda)]$ (2.4348(6) Å),[12c] but longer than that in $[L^1(Cl)GaZn(Cl)(THF)_2]$ (2.3920(6) Å).[12b]

Reactions of $[L^1(Et)GaZnEt]$ (**1b**) with either one equivalent of L^1M (M = Al, Ga) or L^2Si gave $[L^1(Et)GaZnM(Et)L^1]$ (M = Al **2a**, Ga **2b**) and $[L^1(Et)GaZnSi(Et)L^2]$ (**2c**) (Scheme 2) in high yields. Compounds **2a–c** are stable both in the solid and solution states under argon atmosphere. Their ^1H NMR spectra show the characteristic γ-CH proton of L^1 and the Et groups, which are shifted relative to those in **1b**. The ^1H NMR spectrum of **2b** at room temperature displays two distinct quartets at 0.41 and 0.53 ppm for Ga–CH_2CH_3, suggesting restricted rotation of the CH_2 group as confirmed by VT NMR studies. Two quartets were observed at −60 °C, which coalesce into a single broad peak at +70 °C (Fig. S24 and S25). Similarly, the spectrum of **2a** exhibits four different quartets (0.03, 0.12, 0.39, 0.50 ppm) due to the Al–CH_2 and Ga–CH_2 protons. Complexes **1a** and **2a** show broad ^{27}Al NMR resonances at δ 84.76 and 84.13 ppm, indicative of distorted tetrahedral four-coordinate Al atoms. Compound **2c** was isolated as a mixture of diastereomers, evidenced by two sets of proton resonances in the ^1H NMR spectrum (25 °C). The γ-CH proton of L^2, which typically appears as a single resonance, gave two singlets (5.36, 5.39 ppm), and the methylene (=CH_2) protons gave four singlets (3.24, 3.30, 3.97, 4.02 ppm) rather than the expected two for a symmetric environment. VT ^1H NMR studies (25–65 °C) show coalescence of these signals at higher temperatures, indicating a dynamic equilibrium between both diastereomers (Fig. S33 and S34). Similarly, the $^{29}Si\{^1H\}$ NMR shows two peaks at room temperature (−2.23 and −2.81 ppm), which merge into a single resonance (−2.23 ppm) at 65 °C, confirming diastereomer interconversion (Fig. S29 and S32).

Single crystals of compounds **2a–c** were grown from *n*-hexane solutions at −30 °C. Compound **2c** also crystallized from benzene and cyclohexane solution at 25 °C. Crystal structures of these solvates (Table S1; benzene solvate discussed here) were grown to resolve the disorder of the central moiety. However, the outer surfaces of the opposing ends of the molecule are too similar to achieve an ordered packing this way. Considering systematic errors and parameter correlations, all solvates yield comparable results. Complexes **2a–c** crystallises in the monoclinic space group *C*2/*c*. The solid-state structures of **2a–c** are shown in Fig. 3 and Fig. S71–S75.

The Al, Ga, and Si atoms in **2a–c** adopt distorted tetrahedral geometries, whereas the Zn atom is almost linearly coordinated. The Ga1–Zn1 bonds in **2a–c** (2.544(5) Å, 2.4836(2) Å, 2.475(4) Å) are longer than the Ga–Zn bonds in $[\{L^1GaH\}_2Zn]$ (2.4334(12) Å)[12c] and $[(tmeda)Zn\{Ga\{[N(Ar)C(H)]_2\}\}_2]$ (Ar = 2,6-iPr_2-C_6H_3) (2.4491(17) Å, 2.4307(17) Å,[10c] respectively, but comparable to the Ga–Zn bond length of $[\{L^1GaMe\}_2Zn]$ (2.4631(7) Å, 2.4609(7) Å).[12b] The Zn1–Al1 bond of **2a** (2.415(15) Å) is shorter than the Zn–Al bond of $[L^1(Et)AlZnL^3]$ (2.488(1) Å)[3a] and $Zn[Al(\eta^2\text{-}Cp^*)N(SiMe_3)_2]_2$ (2.448(2) Å).[12a] Similarly, the Zn1–Si1 bond of **2c** (2.317(11) Å) is shorter than the Zn–Si bond of $L^2Si(H)–ZnL^1$ (2.4018(9) Å).[18] The Ga1–Zn1–Ga1′ bond angle of **2b** (178.853(16)°) reveals the linear coordination, whereas the Ga–Zn–Ga bond angles in $[\{L^1GaH\}_2Zn]$ (172.68(2)°)[12c] and $[\{L^1GaMe\}_2Zn]$ (173.61(2)°)[12b] deviate larger from linearity. The Ga1–Zn1–Al1 bond angle of **2a** (179.6(3)°) and

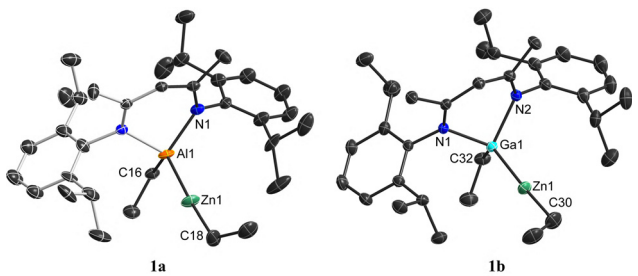

Fig. 2 Molecular structures of **1a–b**. Thermal ellipsoids drawn at 50% probability level. H atoms and the minor component of the disorder are omitted for clarity. Pale coloured part of the molecule is generated *via* symmetry. Selected distances (Å) and angles (°): **1a**: Al1–Zn1 2.4908(10), Zn1–C18 1.983(5), Al1–C16 1.981(4), N1–Al1–N1′ 94.86(12). **1b**: Ga1–Zn1 2.4265(4), Zn1–C30 1.971(3), Ga1–C32 1.986(2), N1–Ga1–N2 92.13(8).

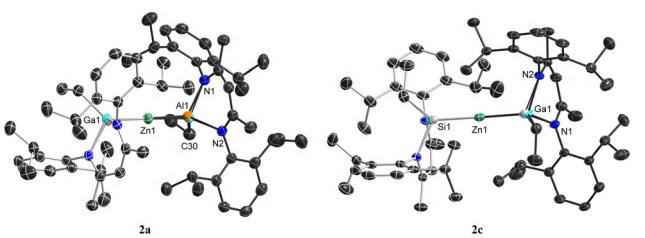

Fig. 3 Molecular structures of **2a** and **2c**. Thermal ellipsoids drawn at 50% probability level. H atoms and solvent molecules are omitted for clarity. The pale-coloured part of the molecule is generated *via* symmetry. Bonds to the minor part of the disorder are displayed thinner. Selected distances (Å) and angles (°): **2a**: Ga1–Zn1 2.544(5), Zn1–Al1 2.415(15), Ga1–Zn1–Al1 179.6(3). **2c** benzene: Ga1–Zn1 2.475(4), Zn1–Si1 (2.317(11), Ga1–Zn1–Si1 174.71(10). See also Table S1.

the Ga1–Zn1–Si1 bond angle of **2c** (174.71(10)°) again show the nearly linear geometry, with **2c** exhibiting a slightly greater deviation.

The reaction of $ZnEt_2$ with L^1Ga (2 equiv.) was monitored by *in situ* ^1H NMR spectroscopy to identify intermediates formed in the synthesis of **2a–c**. Initially, a singlet due to the γ-C*H* proton of **1b** appeared at 4.77 ppm. After 30 minutes, L^1Ga and **1b** were gradually consumed and compound **2b** was formed (singlet at 4.82 ppm). The reaction was finished after 2 h, yielding **2b** exclusively (Fig. S26). These results indicate that **2b** forms *via* stepwise oxidative addition with **1b** as an intermediate.

To further understand the bonding and electronic properties of the binuclear (**1b**) and trinuclear (**2a–c**) compounds, DFT-calculations were conducted at the PBE0/def2-TZVP level of theory.[19] The calculated structure parameters of all compounds agree well with values of the experimental crystal structures (sc-XRD). The HOMO of compound **1b** is located along the Ga–Zn and the Zn–C bonds (Fig. S79), with the main contribution found at the Ga–Zn single bond. The LUMO is found in the backbone of the L^1 ligand. The Ga–Zn bond is identified as a weakened single bond with a Mayer Bond Order (MBO) of 0.77 and a Wiberg Bond Index (WBI) of 0.62. The Ga–Zn bond is polarized towards the Ga atom, as proven by the natural charges of both atoms (Ga = 0.75, Zn = 1.06), with a higher contribution at the Ga atom (62.4%) than the Zn atom (37.6%).

The HOMO of **2a** is located at the Ga–Zn and the Al–Zn bonds, whereas the LUMO is found in the backbone of the L^1Al system. Both the Zn–Ga bond (WBI 0.44) and the Zn–Al bond (WBI 0.55) in **2a** are weaker compared to the Zn–Ga bond in **1b** (Table 1).

Introducing a second L^1Ga molecule in compound **2b** also weakens the Ga–Zn bonds as indicated by the reduced MBO (0.42) and a WBI (0.49) of both Ga–Zn bonds. The HOMO is located along both Ga–Zn bonds, while the LUMO is found in both backbones of the L^1Ga systems. Compound **2c** also shows the HOMO along the Ga–Zn and Zn–Si bonds and the LUMO in the backbone of the L^1Ga system. The Ga–Zn (WBI 0.55) and Zn–Si bonds (WBI 0.41) were identified as weak single bonds. These results are very similar compared to Crimmin's trinuclear complexes $L^1M(ZnCp^*)_2$ (**VIII**) and $L^2Si(ZnCp^*)_2$ (**IX**), for which WBIs of 0.68 (Si), 0.84 (Al) and 0.79 (Ga) were reported.

Preliminary reactivity studies were performed with complex **2c**. **2c** reacted with two equiv. of $B(C_6F_5)_3$ to the zwitterionic compound **3** and adduct **4** ($L^1Ga\rightarrow B(C_6F_5)_2Et$) (Scheme 3), while its reaction with NH_3 gave a mixture of compounds, from

Table 1 Calculated bond orders (MBO, WBI) and natural charges in **1b** and **2a–c**

	1b	2a	2b	2c
MBO (Zn–Ga)	0.77	0.44	0.42/0.42	0.13
MBO (Zn–M)	—	0.74	—	0.85
WBI (Zn–Ga)	0.62	0.44	0.49/0.49	0.55
WBI (Zn–M)	——	0.55	—	0.41
Natural charge (Zn)	1.06	0.78	0.83	0.87
Natural charge (Ga)	0.75	0.70	0.74/0.74	0.77
Natural charge (M)	—	1.01	—	1.20

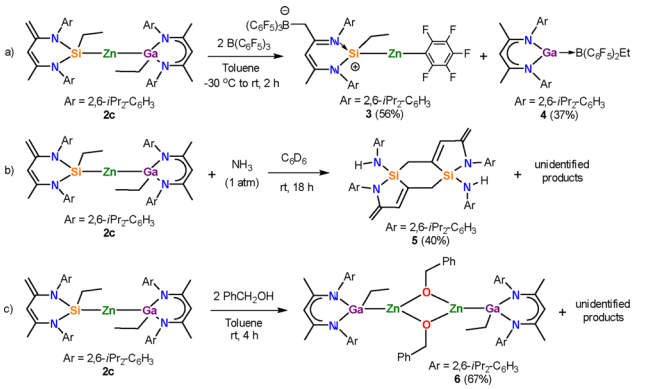

Scheme 3 Synthesis of compounds **3**, **4**, **5**, and **6**.

which **5** was isolated by fractional crystallisation. In addition, **2c** reacted with BnOH to **6** [L^1(Et)GaZn(OCH$_2$Ph)] and additional unidentified by-products (Scheme 3). The ^{29}Si NMR signal of **3** (9.90 ppm) is downfield shifted compared to **2c** (−2.23 ppm) due to the higher positive charge at the Si centre. The ^1H NMR shows a singlet for the γ-CH proton at 6.60 ppm, indicating the presence of an aromatic ring current as reported for {N(Dipp)C(CH$_3$)CHC(CH$_2$B(C$_6$F$_5$)$_3$)(N(Dipp))}Si.[20a] Compound **4** shows a broad ^{11}B singlet (−19.8 ppm) in the typical region of tetracoordinated B atoms and very similar to that of $L^1Ga\rightarrow B(C_6F_5)_3$ (−20.3 ppm),[20b] and the ^1H NMR spectrum shows the γ-CH resonance at 5.04 ppm (Fig. S39–S59). The ^1H NMR spectrum of compound **5** shows two singlets (5.43 ppm) for the γ-CH proton and a singlet at 5.36 ppm for the Ar–NH proton. The ^{29}Si NMR signal of **5** (−20.22 ppm) is upfield shifted compared to that of **2c** (−2.23 ppm). The ^1H NMR spectrum of compound **6** displays a singlet at 4.76 ppm for the γ-CH proton and a singlet at 4.81 ppm corresponding to the OCH$_2$Ph proton.

Compounds **3**, **5**, and **6** crystallize in the triclinic space group $P\bar{1}$ (Fig. 4 and Fig. S76–S78). The Si atom in **3** adopts a distorted tetrahedral geometry and the Zn atom is linearly coordinated.

The Si1–Zn1 bond (2.3508(5) Å) is longer, whereas the Si1–C54 bond (1.8644(14) Å) is shorter than in **2c** (Si–Zn 2.317 Å; Si–C 1.962 Å), consistent with the increased Lewis acidity of the cationic silicon centre. Compound **5** shows a heterotricyclic

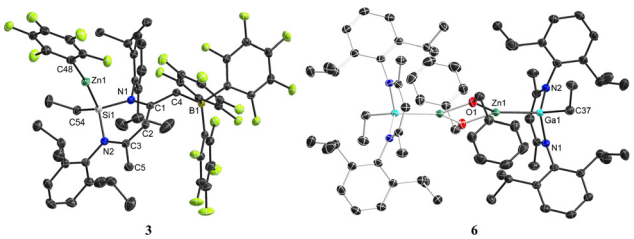

Fig. 4 Molecular structures of **3** and **6**. Thermal ellipsoids drawn at 50% probability level. H atoms and the minor component of the disorder are omitted for clarity. Pale coloured part of the molecule is generated *via* symmetry. Selected distances (Å) and angles (°): **3**: Si1–C3 1.8693(14), Si1–C5 1.8804(14), N1–Si1–N2 111.33(6). **6**: Ga1–Zn1 2.4194(3), Ga1–C37 1.9987(14), Zn1–O1 1.9662(9), N1–Ga1–N2 91.79(4).

framework formed by C–N bond cleavage of L^1. The Si1–C3 (1.8693(14) Å) and Si1–C5 (1.8804(14) Å) bond lengths in **5** are shorter than the Si–C bond length observed in **2c** (1.962 Å). In compound **6**, the Ga1–Zn1 bond length (2.4194(3) Å) is slightly shorter than that in **1b** (2.4265(4) Å), while the Ga1–C37 bond (1.9987(14) Å) is longer than the corresponding Ga–C bond in **1b** (1.986(2) Å).

In summary, heterotrinuclear complexes [L^1(Et)GaZnAl(Et)L^1] (**2a**) and [L^1(Et)GaZnSi(Et)L^2] (**2c**) containing three different metal centres were synthesized by sequential oxidative addition of $ZnEt_2$ to L^1M (M = Al, Ga) and L^2Si *via* intermediate formation of heterobimetallic complexes [L^1(Et)MZnEt] (M = Al **1a**, M = Ga **1b**). The stepwise Zn–Et bond activation was proven by *in situ* ^{1}H NMR spectroscopy, while quantum chemical calculations provided insight into the bonding and electronic structures of **2a–c**. **2c** reacted with $B(C_6F_5)_3$ to the zwitterionic complex **3** and the Lewis acid–base adduct **4**, while compounds **5** and **6** were isolated from reactions with NH_3 and BnOH, respectively. Additional reactivity studies are currently performed.

R. K. Sahoo, investigation (synthesis, characterisation), writing original draft; C. Wölper, investigation (sc-XRD); J. Möbius, investigation (quantum chemical calculations); S. Schulz, resources, supervision, writing – review and editing.

Conflicts of interest

There are no conflicts to declare.

Data availability

The data supporting this article have been included as part of the supplementary information (SI). Supplementry information: experimental procedures, elemental analyses, NMR and IR spectra, crystallographic data and computational details. See DOI: **https://doi.org/10.1039/d5cc03627e**.

CCDC 2467278 (**1a**), 2467279 (**1b**), 2467280 (**2a**), 2467281 (**2b**), 2467282 (**2c** benzene), 2467283 (**2c** cyclohexane), 2467284 (**2c** *n*-hexane), 2482679 (**5**), 2483742 (**3**) and 2487061 (**6**) contain the supplementary crystallographic data for this paper.[21a–j]

Notes and references

1 (*a*) S. T. Liddle, Molecular Metal–Metal Bonds: Compounds, *Synthesis, Properties*, Wiley-VCH, 2015; (*b*) P. Buchwalter, *et al.*, *Chem. Rev.*, 2015, **115**, 28–126.
2 (*a*) P. Kalck, *Homo- and Heterobimetallic Complexes in Catalysis: Cooperative Catalysis*, Springer International Publishing, Cham, 2016, vol. 59; (*b*) N. Wheatley and P. Kalck, *Chem. Rev.*, 1999, **99**, 3379–3420; (*c*) S. D. Robertson, *et al.*, *Chem. Rev.*, 2019, **119**, 8332–8405; (*d*) J. Campos, *Nat. Rev. Chem.*, 2020, **4**, 696–702; (*e*) J. M. Gil-Negrete and E. Hevia, *Chem. Sci.*, 2021, **12**, 1982–1992; (*f*) H.-C. Yu and N. P. Mankad, *Synthesis*, 2021, 1409–1422.
3 (*a*) C. Bakewell, *et al.*, *Chem. Sci.*, 2018, **9**, 2348–2356; (*b*) S. Brand, *et al.*, *Angew. Chem., Int. Ed.*, 2019, **58**, 15496–15503; (*c*) M. J. Evans, *et al.*, *Chem. Commun.*, 2022, **58**, 10091–10094; (*d*) F. Dankert and E. Hevia, *Chem. – Eur. J.*, 2024, **30**, e202304336.
4 O. Kysliak, *et al.*, *J. Am. Chem. Soc.*, 2021, **143**, 142–148.
5 A. Friedrich, *et al.*, *Angew. Chem., Int. Ed.*, 2021, **60**, 16492–16499.
6 (*a*) R. J. Baker and C. Jones, *Coord. Chem. Rev.*, 2005, **249**, 1857–1869; (*b*) A. Kempter, *et al.*, *Inorg. Chem.*, 2008, **47**, 7279–7285; (*c*) S. Gonzalez-Gallardo, *et al.*, *Met. Bonding*, 2010, 147–188; (*d*) K. Yurkerwich, *et al.*, *Chem. Sci.*, 2010, **1**, 210–214; (*e*) G. Linti and T. Zessin, *Dalton Trans.*, 2011, **40**, 5591–5598; (*f*) S. González-Gallardo, *et al.*, *Chem. Rev.*, 2012, **112**, 3136–3170; (*g*) D. Mukherjee, *Aluminium and Galium, Comprehensive Coordination Chemistry III*, ed.E. C. Constable, G. Parkin and L. Que Jr, Elsevier, Oxford, 2021, pp. 197–213; (*h*) B. Rösch, *et al.*, *Nature*, 2021, **592**, 717–721; (*i*) A. Caise, *et al.*, *Chem. Commun.*, 2023, **59**, 7251–7254; (*j*) A. Barthélemy and I. Krossing, *Inorg. Chem.*, 2024, **63**, 21763–21787; (*k*) R. Yamanashi, *et al.*, *Chem. – Eur. J.*, 2025, **31**, e202501315.
7 A. Schnepf and C. Doriat, *Chem. Commun.*, 1997, 2111–2112.
8 D. Dhara, *et al.*, *J. Am. Chem. Soc.*, 2024, **146**, 33536–33542.
9 J. Hicks, *et al.*, *Angew. Chem., Int. Ed.*, 2015, **54**, 10000–10004.
10 (*a*) M. Zhong, *et al.*, *Dalton Trans.*, 2020, **49**, 1351–1364; (*b*) C. Gemel, *et al.*, *Eur. J. Inorg. Chem.*, 2004, 4161–4176; (*c*) C. Jones, *et al.*, *Dalton Trans.*, 2007, 2997–2999; (*d*) G. Prabusankar, *et al.*, *Eur. J. Inorg. Chem.*, 2010, 4415–4418; (*e*) C. Ganesamoorthy, *et al.*, *Nat. Commun.*, 2018, **9**, 87; (*f*) C. Helling, *et al.*, *Chem. – Eur. J.*, 2020, **26**, 13390–13399; (*g*) Y. Cai, *et al.*, *J. Am. Chem. Soc.*, 2022, **144**, 16647–16655; (*h*) G. Feng, *et al.*, *J. Am. Chem. Soc.*, 2024, **146**, 7204–7209; (*i*) L. P. Griffin, *et al.*, *Angew. Chem., Int. Ed.*, 2024, **63**, e202405053.
11 C. Ganesamoorthy, *et al.*, *Organometallics*, 2015, **34**, 2991–2996.
12 (*a*) J. Weßing, *et al.*, *Inorg. Chem.*, 2017, **56**, 3517–3525; (*b*) A. Kempter, *et al.*, *Inorg. Chem.*, 2007, **46**, 9481–9487; (*c*) L. J. Morris, *et al.*, *Chem. – Eur. J.*, 2022, **28**, e202201480.
13 (*a*) W. Yang, *et al.*, *Nat. Synth.*, 2025, **4**, 995–1000; (*b*) K. Freitag, *et al.*, *Angew. Chem., Int. Ed.*, 2015, **54**, 4370–4374; (*c*) S. Jiang, *et al.*, *Inorg. Chem.*, 2022, **61**, 8083–8089.
14 M. P. Blake, *et al.*, *Chem. Commun.*, 2015, **51**, 5743–5746.
15 C. Cui, *et al.*, *Angew. Chem., Int. Ed.*, 2000, **39**, 4274–4276.
16 N. J. Hardman, *et al.*, *Chem. Commun.*, 2000, 1991–1992.
17 A. Paparo, *et al.*, *Angew. Chem., Int. Ed.*, 2019, **58**, 11459–11463.
18 B. Li, *et al.*, *Organometallics*, 2023, **42**, 457–464.
19 (*a*) C. Adamo, *et al.*, *J. Mol. Struct. Theochem*, 1999, **493**, 145–157; (*b*) F. Weigend and R. Ahlrichs, *Phys. Chem. Chem. Phys.*, 2005, **7**, 3297–3305; (*c*) F. Neese, *WIREs Comput. Mol. Sci.*, 2012, **2**, 73–78; (*d*) F. Neese, *WIREs Comput. Mol. Sci.*, 2022, **12**, e1606.
20 (*a*) M. Driess, *et al.*, *Angew. Chem., Int. Ed.*, 2006, **45**, 6730–6733; (*b*) N. J. Hardman, *et al.*, *Chem. Commun.*, 2001, 1866–1867.
21 (*a*) CCDC 2467278: Experimental Crystal Structure Determination, 2025, DOI: **10.5517/ccdc.csd.cc2ntdmj**; (*b*) CCDC 2467279: Experimental Crystal Structure Determination, 2025, DOI: **10.5517/ccdc.csd.cc2ntdnk**; (*c*) CCDC 2467280: Experimental Crystal Structure Determination, 2025, DOI: **10.5517/ccdc.csd.cc2ntdpl**; (*d*) CCDC 2467281: Experimental Crystal Structure Determination, 2025, DOI: **10.5517/ccdc.csd.cc2ntdqm**; (*e*) CCDC 2467282: Experimental Crystal Structure Determination, 2025, DOI: **10.5517/ccdc.csd.cc2ntdrn**; (*f*) CCDC 2467283: Experimental Crystal Structure Determination, 2025, DOI: **10.5517/ccdc.csd.cc2ntdsp**; (*g*) CCDC 2467284: Experimental Crystal Structure Determination, 2025, DOI: **10.5517/ccdc.csd.cc2ntdtq**; (*h*) CCDC 2482679: Experimental Crystal Structure Determination, 2025, DOI: **10.5517/ccdc.csd.cc2pbffx**; (*i*) CCDC 2483742: Experimental Crystal Structure Determination, 2025, DOI: **10.5517/ccdc.csd.cc2pcjqb**; (*j*) CCDC 2487061: Experimental Crystal Structure Determination, 2025, DOI: **10.5517/ccdc.csd.cc2pgzsy**.